



Cite this: *RSC Adv.*, 2019, 9, 11589

# One-dimensional facile growth of MAPbI<sub>3</sub> perovskite micro-rods

Arti Mishra,<sup>a</sup> Zubair Ahmad,<sup>b</sup> Farid Touati,<sup>a</sup> R. A. Shakoor<sup>b</sup> and Mohammad Khaja Nazeeruddin<sup>c</sup>

One-dimensional microrods (4–5 μm) of PbI<sub>2</sub> and CH<sub>3</sub>NH<sub>3</sub>PbI<sub>3</sub> (MAPbI<sub>3</sub>) with unique structural and morphological properties have been grown at room temperature. X-ray diffraction (XRD) patterns of both types of micro-rods exhibit a hexagonal system (*P* $\bar{3}$ *m*1(164) space group) with 2H polytype structures. In the case of PbI<sub>2</sub>, the atomic composition of the microcrystals indicates the formation of pure phases of PbI<sub>2</sub>, however, energy-dispersive X-ray spectroscopy (EDX) of MAPbI<sub>3</sub> indicates the existence of intermediate phases due to the addition of MAI. FTIR results reveal the existence of a strong interaction between C–H and N–H groups in the crystals which has been cross validated by Raman spectroscopic analysis. The morphological studies performed by scanning electron microscopy (SEM) and transmission electron microscopy (TEM) confirm the crack free morphology of PbI<sub>2</sub> and MAPbI<sub>3</sub> micro-rods with a porous structure. Thermogravimetric analysis (TGA) and differential scanning calorimetry (DSC) studies show that the addition of MAI in the PbI<sub>2</sub> reduced the weight loss and the decomposition temperature has been increased by 1.5 °C as well. The growth of these unique one-dimensional micro-rods signifies a novel concept in perovskite synthesis for solar cells and optoelectronic applications.

Received 9th January 2019

Accepted 8th April 2019

DOI: 10.1039/c9ra00200f

rsc.li/rsc-advances

## 1 Introduction

The crystal structure of a material provides precise information about phase purity, the connectivity of the atoms, the bond distances and angles between these atoms. It also provides inter and intra molecular interactions which may provide insight into the chemistry and properties of the compound. The shape and size of crystals have profound impacts on electrical and optical properties. Crystals contain fewer heterostructure defects and deliver better electronic, mechanical, optical and transport properties, and hence are technologically more suitable in diversified engineering and medical applications.<sup>1</sup> The shape of the crystals varies from three-dimensional large sized crystals, two-dimensional nanoplates, and one-dimensional nanowires to zero-dimensional quantum dots. Among the 2D crystals,<sup>2</sup> the semiconductors and specifically the organic/inorganic metal halide (OMH) family are more pertinent to electronic and optoelectronic devices due to their good intrinsic properties such as optical bandgap, absorption coefficient and carrier diffusion length.<sup>3,4</sup> The lead-based OMHs have gained great attention by virtue of their use in solar cells and optoelectronic applications.

The carrier diffusion length measured in three-dimensional perovskite is strongly dependent on material morphology and crystalline structure.<sup>5</sup> However, one-dimensional perovskite crystals are not thoroughly explored. Many questions remain to be addressed regarding the one dimensional chemistry and the nature of charge transfer in the one dimensional perovskite materials.<sup>6</sup> The understanding and study of all above stated fundamental intrinsic properties are necessary for further improvement of the functions of one-dimensional perovskites. In this context, we performed solution-based facile synthesis of PbI<sub>2</sub> and MAPbI<sub>3</sub> perovskite one-dimensional micro-rods. The morphological, structural and thermal properties of the one-dimensional perovskite micro-rods have been examined using various characterization techniques. To the best of our knowledge, this is the first report on the millimeter scale PbI<sub>2</sub> and MAPbI<sub>3</sub> one-dimensional microcrystalline rods of such morphological and structural characteristics.

## 2 Materials and methods

Lead(II) iodide (PbI<sub>2</sub>) and methylammonium iodide (MAI) were purchased from Sigma-Aldrich, TCI Chemicals (Japan), respectively. Dimethylformamide DMF (anhydrous, 99.8%) and isopropanol (IPA) were supplied by Agros chemicals and VWR Prolab chemicals. All the chemicals were used as received without any further purification. In order to prepare the one-dimensional micro-rods, 1 M solutions of PbI<sub>2</sub> and MAI were prepared separately in DMF and IPA, respectively. Then the PbI<sub>2</sub>

<sup>a</sup>Department of Electrical Engineering, College of Engineering, Qatar University, P. O. Box 2713, Doha, Qatar

<sup>b</sup>Center for Advanced Materials (CAM), Qatar University, P. O. Box 2713, Doha, Qatar. E-mail: zubairtarar@qu.edu.qa; Tel: +974-4403-7729

<sup>c</sup>Group for Molecular Engineering of Functional Materials, Institute of Chemical Sciences and Engineering, École Polytechnique Fédérale de Lausanne, CH-1951 Sion, Switzerland



and MAI solutions were mixed in the 2 : 1 volumetric ratio and the thick precipitates in the perovskite's solution were formed. However, simultaneous heating and stirring at 70 °C gives a clear yellow solution of the MAPbI<sub>3</sub>. The solutions of PbI<sub>2</sub> and MAPbI<sub>3</sub> was left to cool down slowly at a very slow rate (@10 °C/HR) and the growth of the micro-rods were observed after many hours of cooling down solution to room temperature. The length of micro rod is increasing if the solution has been kept for few days without shaking. Fig. 1 show the SEM image and photos of the crystals grown in the solution of the PbI<sub>2</sub>.

The surface morphology of the one-dimensional micro rods was investigated using JEOL 7600 scanning electron microscope while the thermal stability of the prepared micro-rods was studied by thermogravimetric analysis (TGA) and differential scanning calorimetry (DSC). TGA and DSC analyses were undertaken by PerkinElmer TGA 4000 Analyzer and PerkinElmer DSC 8500 instruments under nitrogen environment, respectively. The Raman spectra were obtained by using Jobin-Yvon HR800 UV-Vis-NIR, Raman spectrometer equipped with an Olympus BX 40 attachment. The excitation wavelength was 514.5 nm with an energy setting of 1.2 mW were employed from a coherent argon-ion laser (Innova, model 308). The Raman spectra were recorded by means of back scattering geometry with an acquisition time of 50 seconds. Fourier transform infrared spectroscopy was performed using, PerkinElmer (Spectrum 2000, USA) over the wave number range 4000–400 cm<sup>-1</sup>. X-ray diffraction (XRD) patterns were recorded using EMPYREAN diffractometer operated at 45 kV, 40 mA with K $\alpha$ 1 and K $\alpha$ 2 radiations having 1.540598 Å and 1.544426 Å wavelength, respectively, with a scan speed of 1 s per step and a step size of 0.013° 2 $\theta$ .

### 3 Results and discussion

Fig. 2(a–f) shows the morphology of the prepared microcrystalline rods at different magnification. The morphological examination of Fig. 2(a and d) indicates that the micro crystals grow in longitudinal dimension having lengths up to 5 mm. Furthermore, it can also be seen that the lateral dimensions of the microcrystals are of 10–100  $\mu$ m diameter. The SEM images

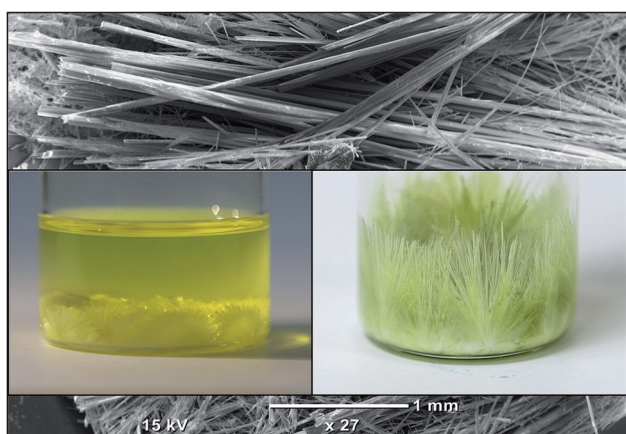


Fig. 1 SEM image and photos of the PbI<sub>2</sub> crystals grown in the DMF solution.

also reveal that the microcrystals of PbI<sub>2</sub> (Fig. 2(b and c)) and MAPbI<sub>3</sub> (Fig. 2(e and f)) contain pores having a size in the submicron range. The higher magnification image of the microcrystal show that many parallel nanowires are joined longitudinally to form a large micro-rod. Due to slight differences in the dimensions of the nanowires, they've left a small space between adjacent wires while joining together which results in the formation of hallow regions. However, no adjacent cracks have also been observed on the microcrystalline rods at lower magnification which can be regarded as there is no visual defect during the joining of two or more crystalline wires.

The compositional analysis of the developed microcrystals has been performed using EDS and the results are shown in Fig. 3(a and b). For all crystals the EDS spectra show well defined peaks corresponding to elements such as carbon lead and iodine. There are two feature peaks at 2.32 and 10.5 keV corresponding to the lead and two feature peaks at 3.98 and 4.2 keV which can be assigned to iodine elements in PbI<sub>2</sub> crystals. In the case of PbI<sub>2</sub>, the atomic composition of the microcrystals indicates the presence of Pb with I in a 1 : 2.1 ratio, which is in close agreement with the PbI<sub>2</sub>, confirming the formation of pure phases. However, in the case of MAPbI<sub>3</sub>, this ratio is turned to 1 : 1.5. This might be due to the existence of separate phases of PbI<sub>2</sub> and MAI. Here it is also important to note that the MAPbI<sub>3</sub> has been extremely sensitive to high energy electron beam radiation and thus it is easy to decompose into PbI<sub>2</sub> during EDS measurement.<sup>7</sup>

In order to have more insight of the developed microcrystals of PbI<sub>2</sub> and MAPbI<sub>3</sub>, HRTEM analysis was conducted and the results are presented in Fig. 4(a and b). TEM images taken from the selected region to show the further existence of the nanopores in the micro-rods and no cracks are observed in a microcrystal surface. Further high-resolution TEM images of PbI<sub>2</sub> MAPbI<sub>3</sub> crystals cannot be obtained because the PbI<sub>2</sub> and MAPbI<sub>3</sub> crystals are sensitive to high-energy electron beam irradiation, which can cause distortion of their crystal structure.

X-ray diffraction spectra of synthesized one-dimensional crystals are shown in Fig. 5. For a clear comparison, the XRD spectra of the starting materials in powder form, commercially purchased from Sigma-Aldrich, is also included as shown in Fig. 5(a and b). Fig. 5(a) corresponds to the XRD spectrum of the PbI<sub>2</sub> crystal (yellow circles) and commercially purchased PbI<sub>2</sub> powder (black lines). Both XRD patterns showed a hexagonal system (*P*3*m*1(164) space group) with *a* = *b* = 0.4557 nm and *c* = 0.6979 of PbI<sub>2</sub> and 2H polytype structure (hematite, JCPDS file no. 07-0235).<sup>8</sup> The most intense diffraction peak is obtained at 12.60° that corresponds to the (001) lattice plane. However, the peak intensity at this angle for PbI<sub>2</sub> crystal is much higher than the PbI<sub>2</sub> powder. Other prominent peaks are observed at 25.5°, 25.93°, 34.2°, 38.67° and 52.3° corresponding to the (002), (011), (102), (003), and (004) lattice planes of PbI<sub>2</sub>. Some other preferential orientation peaks of PbI<sub>2</sub> corresponding to (113), and (114) planes are observed at higher diffraction angles 56.4° and 67.5°, respectively as indicated in the Fig. 5(a). The crystalline orientations obtained in the present work are different from those of previous literatures for MAPbI<sub>3</sub> films as well as bulk crystals.<sup>9,10</sup> In the prepared crystals, the *d*-spacing is fingerprints of specific sample that is determined by XRD. It can be noticed



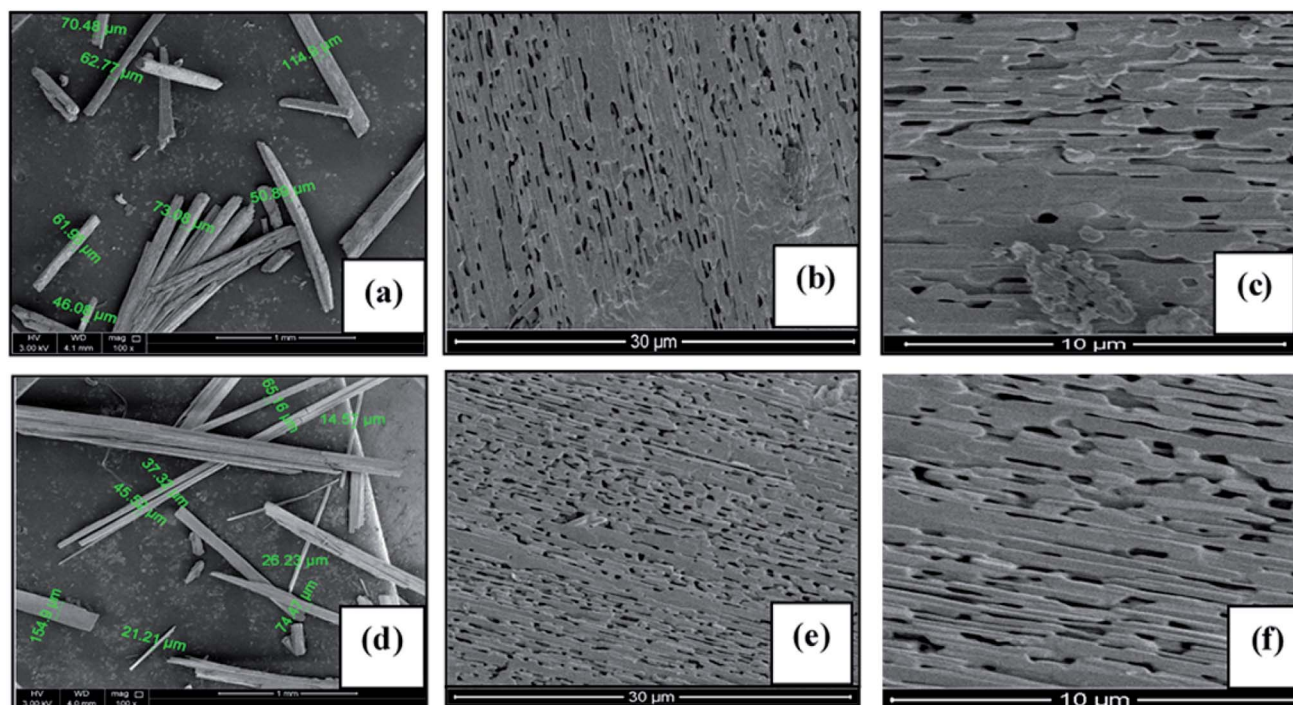


Fig. 2 FESEM images of the  $\text{PbI}_2$  and  $\text{MAPbI}_3$  the micro-rods taken at different magnification. (a–c) represents the  $\text{PbI}_2$  while the (d–f) denotes the  $\text{MAPbI}_3$ .

that the  $d$ -spacing of the  $\text{PbI}_2$  crystal is more as compared to  $\text{PbI}_2$  powder resulting in shifting of the lattice planes towards lower angles. The shifting of plane spacing ( $d$ -value) may be due to rearrangement of lattice positions.<sup>11</sup>

Similarly, the  $\text{MAPbI}_3$  one dimensional crystals have adopted the hexagonal structure with  $P\bar{3}m1(164)$  space group. High intensity diffraction peaks are obtained at lower angle positions  $9.0^\circ$ ,  $9.5^\circ$ ,  $18.1^\circ$  and  $24.5^\circ$  (Fig. 5(b)) overwhelmingly dominate the diffraction pattern. The high intensity diffraction peaks confirm the high crystalline nature of the prepared phase. The same  $c$ -axis diffraction peaks obtained in  $\text{PbI}_2$  powder at (002),

(003), and (004) are also obtained in  $\text{MAPbI}_3$  crystals at angles  $12.67^\circ$ ,  $19.05^\circ$ , and  $25.5^\circ$  respectively with very poor intensities. Intense diffraction peaks respectively assigned to (110), (202), (004) and (220) confirms the  $\text{MAPbI}_3$  phase. Furthermore few low intensity marker of  $\text{MAPbI}_3$  phase is also present at (310), (314), and (404).<sup>12</sup> The unidentified peaks representing stable phase at the room temperature did not match either the pure  $\text{PbI}_2$  or MAI phase. This suggests a new intermediate phase, which might be a complex of  $\text{PbI}_2$ –DMF or complex of  $\text{PbI}_2$ –MAI–DMF.<sup>13</sup>

The structure of the synthesized one-dimensional micro-crystals has also been examined by the FTIR and the results are shown in Fig. 6. The FTIR vibrations at  $660$  and  $860\text{ cm}^{-1}$  show the features characteristic of C–O stretching and C–N stretching. The absorption peak at  $840\text{ cm}^{-1}$  produced by e bending vibration peak of  $\text{CH}_3$ . Peaks at  $1007$ ,  $1058\text{ cm}^{-1}$  belongs to  $\text{sp}^3$  C–H stretching. Signal around  $2900\text{ cm}^{-1}$ , that is a strong marker of the presence of this group are weak here, but they are very prominent in RAMAN. Peaks between  $1250$ – $1550\text{ cm}^{-1}$  of the frequency of vibration belongs to C–H and N–H bending. However, overshoots at  $1265$  and  $1385\text{ cm}^{-1}$  is not visible in  $\text{MAPbI}_3$ . The stretching vibration due to C=O bond appeared at  $1620\text{ cm}^{-1}$  and at  $1660\text{ cm}^{-1}$  (this group is present in the DMF molecule as well). However, the C=O bond strength decreased with the MAI addition in  $\text{PbI}_2$ . It has been observed that there are no O–H stretching vibrations around  $3500\text{ cm}^{-1}$  suggesting absence of hydrated or adsorbed water.<sup>14,15</sup> The O–H oscillations of water molecules are embedded in such a way that they affect the hydrogen bonds between the N–H group and the iodide because the N–H stretch vibrations are known for their sensitivity to the strength of the interaction between the

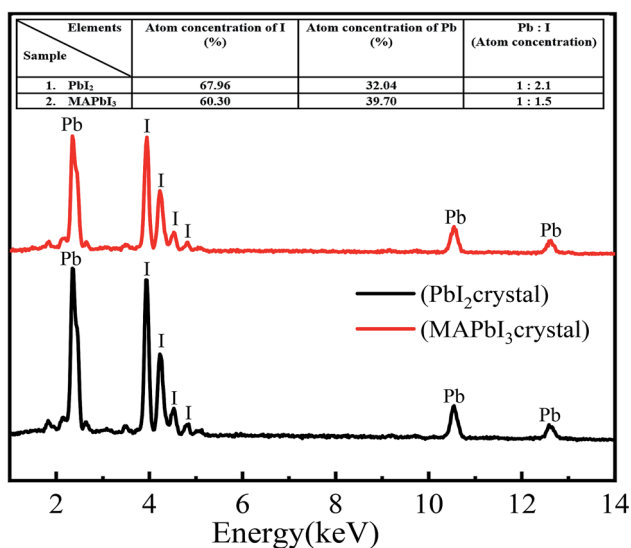


Fig. 3 EDS spectra of the micro-rods:  $\text{PbI}_2$  and  $\text{MAPbI}_3$ .



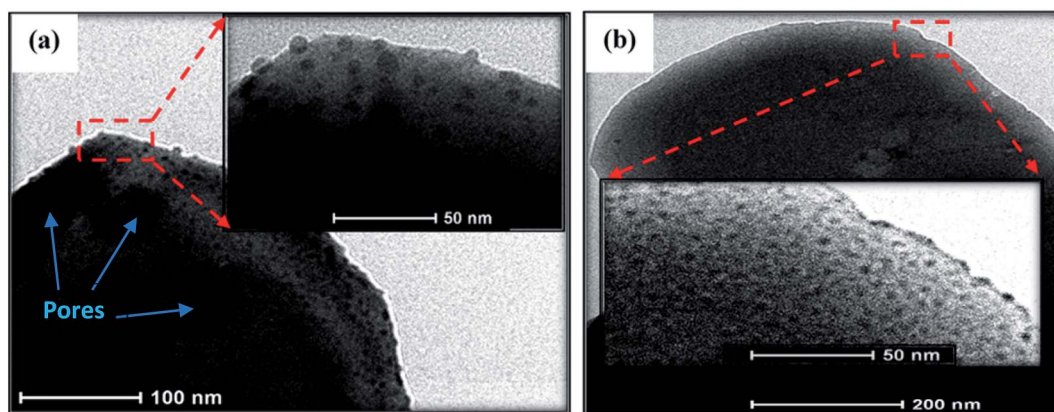


Fig. 4 TEM images for crystal rods  $\text{PbI}_2$  (a),  $\text{MAPbI}_3$  (b), insets shows higher magnification images of same surface.

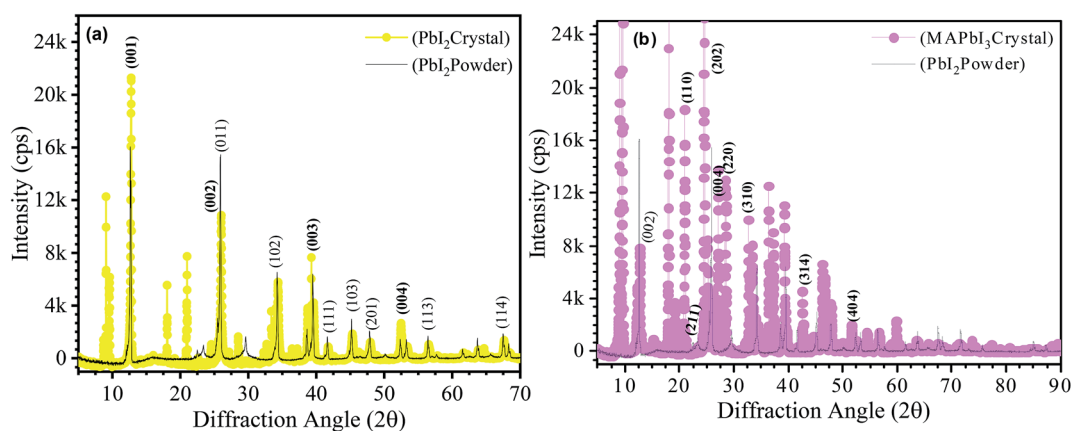


Fig. 5 Diffraction patterns of  $\text{PbI}_2$  powder,  $\text{PbI}_2$  crystals and  $\text{MAPbI}_3$  micro crystalline rods recorded at room temperature. (a)  $\text{PbI}_2$  crystal (yellow data points) and  $\text{PbI}_2$  powder (black line). (b)  $\text{MAPbI}_3$  crystal (magenta data points) and  $\text{PbI}_2$  powder (black line).

methylammonium and the iodide. Even though, the MAI is not present in the solutions except  $\text{MAPbI}_3$  but C–H and N–H stretching and bending vibrations are very similar for all the dry crystals. The FTIR peaks in the  $500\text{--}1700\text{ cm}^{-1}$  range are well correspond to the Raman features as shown in Fig. 7. Though,

some peaks cannot be found in the infrared spectra, but are present in the Raman spectra precisely above  $1700\text{ cm}^{-1}$ . This is because of the fact that the vibrational energy in Raman is active due to changes in polarization whereas IR active intensities are depending on the dipole moment.<sup>16,17</sup>

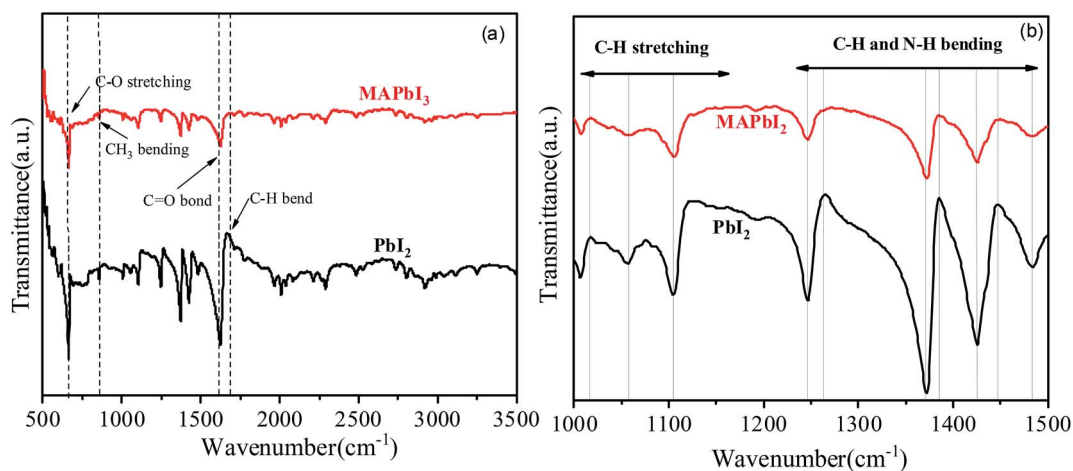


Fig. 6 FTIR spectra of  $\text{PbI}_2$  and  $\text{MAPbI}_3$  micro-rods: (a)  $500\text{--}3500\text{ cm}^{-1}$  and (b)  $1100\text{--}1500\text{ cm}^{-1}$ .



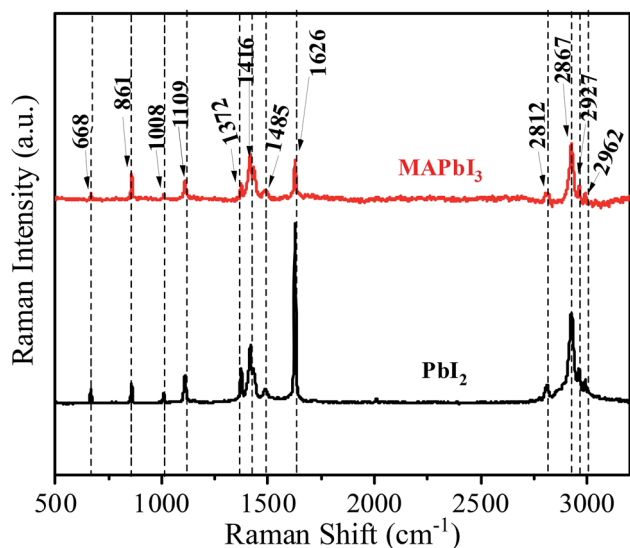


Fig. 7 Raman spectra of  $\text{PbI}_2$  and  $\text{MAPbI}_3$  one dimensional micro-rods.

Raman spectroscopic analysis of the prepared materials is presented in Fig. 7. Characteristic internal vibrations appear at three energetic regions; (i) the C–N stretching at  $600\text{--}1100\text{ cm}^{-1}$ , (ii)  $\text{CH}_3$  and  $\text{NH}_3$  bending around  $1300\text{--}1600\text{ cm}^{-1}$  and (iii)  $\text{CH}_3$  and  $\text{NH}_3$  is stretching at around  $3000\text{ cm}^{-1}$ . Qualitatively, each  $\text{PbI}_2$  and  $\text{MAPbI}_3$  shows similar vibrational properties with three energetic regions, hence there is no phase transformation/change during the crystallization process. These ranges are consistent with previous reports.<sup>18–20</sup>

Thermogravimetric analysis (TGA) is used to determine the thermal stability of the micro-rods and the results are presented in Fig. 8. It can be noticed that weight loss is observed in two

temperature ranges; (i) between  $110\text{--}116\text{ }^\circ\text{C}$  showing weight loss less than 15% for all samples. Minimum (12%) mass loss is obtained in  $\text{PbI}_2$  crystal at  $110.83\text{ }^\circ\text{C}$  and maximum (15%) is in  $\text{MAPbI}_3$  micro-rods at  $115.87\text{ }^\circ\text{C}$ . The TGA weight loss profile implies that these materials have not undergone thermal decomposition or sublimation during 1<sup>st</sup> stage and mass loss is solely due to the removal of absorbed moisture from the microcrystals. Because sublimation has been defined as the point where at least 20% of mass loss of the sample has happened.<sup>21</sup> The 2<sup>nd</sup> weight loss is observed between  $550\text{ }^\circ\text{C}$  and  $600\text{ }^\circ\text{C}$  for the synthesized crystals. This sequential decomposition is observed in the perovskite materials where organic component decomposes by the subsequent mass loss of HI and  $\text{CH}_3\text{NH}_2$  because the latter species is more tightly incorporated in the perovskite matrix. Sequential decomposition pathway occurs only when the organic species are combined into the perovskite structure. This type of decomposition is not observed in the pure  $\text{PbI}_2$  and MAI powder.  $\text{PbI}_2$  powder (99% pure) undergoes 90% weight loss at  $646\text{ }^\circ\text{C}$  and MAI undergoes 100% weight loss at  $185\text{ }^\circ\text{C}$  (ref. 22) which means pure organic material and inorganic material shows single step mass loss decomposition behavior. This single step loss is not observed in the TGA of all the crystal samples. Thermal behavior of prepared microcrystals is in a good agreement with the previous results.<sup>22,23</sup> DSC was also used to effectively detect phase transitions and to gain further insight into the thermal behavior of the microcrystals. The heating-cooling cycle DSC measurements over the temperature range of  $50\text{--}200\text{ }^\circ\text{C}$  has been carried out and corresponding results are shown in the inset of Fig. 8. A narrow endothermic peaks in a temperature range of  $125\text{--}132\text{ }^\circ\text{C}$  is noticed which can be ascribed to the polymorphic transformation while heating.<sup>24</sup>

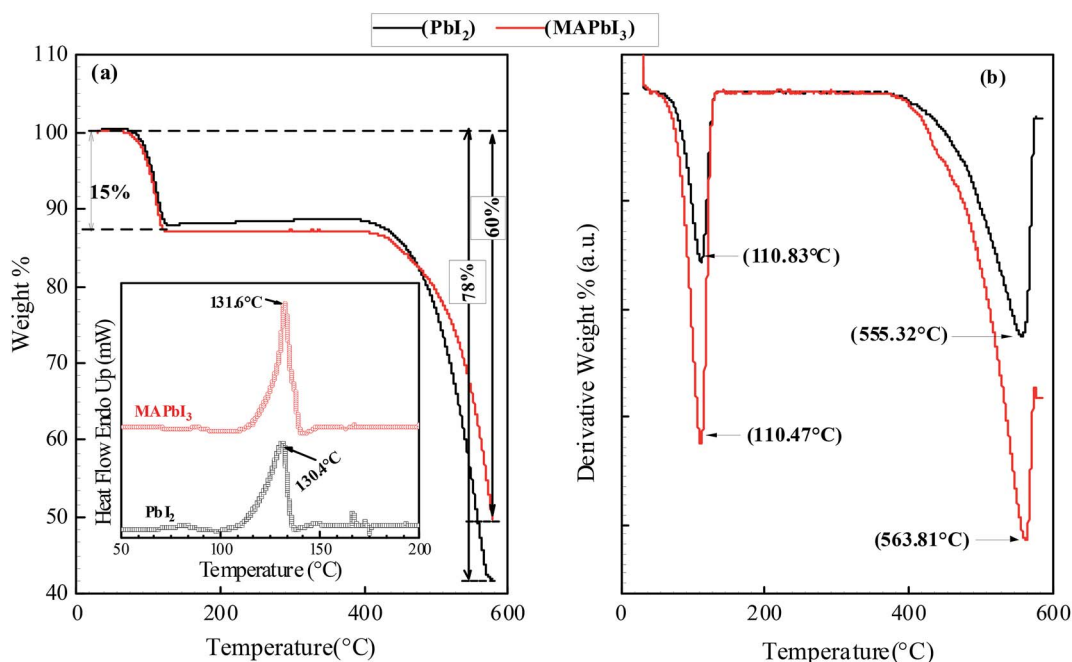


Fig. 8 TGA heating curves of individual crystals expressed as (a) weight% and its (b) derivatives as a function of applied temperature. Inset shows the DSC heating curves for the  $\text{PbI}_2$  and  $\text{MAPbI}_3$  micro-rods.



## 4 Conclusions

In summary, facial growth of one-dimensional  $\text{PbI}_2$  and  $\text{MAIPbI}_3$  based perovskite micro rods has been undertaken. The morphological, structural and thermal properties of the one-dimensional perovskite micro-rods have been examined using various characterization techniques. X-ray diffraction and SEM/EDX analyses confirm phase purity and high crystallinity of the developed micro-rods. Thermal analysis (TGA) indicates decent thermal stability of  $\text{PbI}_2$  and  $\text{MAIPbI}_3$  microcrystals. The decomposition of  $\text{PbI}_2$  microcrystals observed in the temperature of 500–600 °C is in good agreement with the thermal decomposition of the one-dimensional perovskites. FTIR and Raman spectroscopy analyses confirm the existence of strong interactions between different stable groups in the crystals. The morphological studies (SEM/TEM) confirm crack free morphology of  $\text{PbI}_2$  and  $\text{MAPbI}_3$  micro-rods with porous structure. The micro-rods of  $\text{PbI}_2$  and  $\text{MAPbI}_3$  may be considered for the application in perovskites photovoltaics and beyond. Hence, the development of these unique one-dimensional micro-rods represents a novel concept in materials design and synthesis that may foster ground-breaking research.

## Conflicts of interest

The authors declare that there is no conflict of interest.

## Acknowledgements

This work is supported by Qatar University Internal Grant No. QUCG-CAM-2018/19-1. The findings achieved herein are solely the responsibility of the authors. The authors also acknowledge the Qatar National Library for providing the financial support to pay open access charges for this publication.

## References

- 1 S. Tongay, Preface to a Special Topic: 2D Materials and Applications, *Appl. Phys. Rev.*, 2018, 5(1), 010401.
- 2 G. R. Bhimanapati, *et al.*, Recent Advances in Two-Dimensional Materials beyond Graphene, *ACS Nano*, 2015, 9(12), 11509–11539.
- 3 V. Kaushik, *et al.*, Scalable Exfoliation of Bulk  $\text{MoS}_2$  to Single- and Few-Layers Using Toroidal Taylor Vortices, *Nanomaterials*, 2018, 8(8), 587.
- 4 L. Yang, *et al.*, Properties, Preparation and Applications of Low Dimensional Transition Metal Dichalcogenides, *Nanomaterials*, 2018, 8(7), 463.
- 5 J. Huang, Y. Shao and Q. Dong, Organometal Trihalide Perovskite Single Crystals: A Next Wave of Materials for 25% Efficiency Photovoltaics and Applications Beyond?, *J. Phys. Chem. Lett.*, 2015, 6(16), 3218–3227.
- 6 P.-A. Mante, *et al.*, Electron–acoustic phonon coupling in single crystal  $\text{CH}_3\text{NH}_3\text{PbI}_3$  perovskites revealed by coherent acoustic phonons, *Nat. Commun.*, 2017, 8, 14398.
- 7 S. Chen, *et al.*, Atomic scale insights into structure instability and decomposition pathway of methylammonium lead iodide perovskite, *Nat. Commun.*, 2018, 9(1), 4807.
- 8 P. E. Tomaszewski, Structural phase transitions in crystals. I. Database, *Phase Transitions*, 1992, 38(3), 127–220.
- 9 Y. Fu, *et al.*, Solution growth of single crystal methylammonium lead halide perovskite nanostructures for optoelectronic and photovoltaic applications, *J. Am. Chem. Soc.*, 2015, 137(17), 5810–5818.
- 10 M. Xiao, *et al.*, A fast deposition-crystallization procedure for highly efficient lead iodide perovskite thin-film solar cells, *Angew. Chem., Int. Ed. Engl.*, 2014, 53(37), 9898–9903.
- 11 P. Beckmann, ChemInform Abstract: A Review of Polytypism in Lead Iodide, *Cryst. Res. Technol.*, 2010, 45, 455–460.
- 12 T. Baikie, *et al.*, Synthesis and crystal chemistry of the hybrid perovskite  $(\text{CH}_3\text{NH}_3)\text{PbI}_3$  for solid-state sensitised solar cell applications, *J. Mater. Chem. A*, 2013, 1(18), 5628–5641.
- 13 B. R. Vincent, *et al.*, Alkylammonium lead halides. Part 1. Isolated  $\text{PbI}_6^{4-}$  ions in  $(\text{CH}_3\text{NH}_3)_4\text{PbI}_6 \cdot 2\text{H}_2\text{O}$ , *Can. J. Chem.*, 1987, 65(5), 1042–1046.
- 14 J. Idígoras, *et al.*, The interaction between hybrid organic–inorganic halide perovskite and selective contacts in perovskite solar cells: an infrared spectroscopy study, *Phys. Chem. Chem. Phys.*, 2016, 18(19), 13583–13590.
- 15 M. A. Pérez-Osorio, *et al.*, Vibrational Properties of the Organic–Inorganic Halide Perovskite  $\text{CH}_3\text{NH}_3\text{PbI}_3$  from Theory and Experiment: Factor Group Analysis, First-Principles Calculations, and Low-Temperature Infrared Spectra, *J. Phys. Chem. C*, 2015, 119(46), 25703–25718.
- 16 N. Ahn, *et al.*, Highly Reproducible Perovskite Solar Cells with Average Efficiency of 18.3% and Best Efficiency of 19.7% Fabricated via Lewis Base Adduct of Lead(II) Iodide, *J. Am. Chem. Soc.*, 2015, 137(27), 8696–8699.
- 17 E. Mosconi, *et al.*, Structural and electronic properties of organo-halide lead perovskites: a combined IR-spectroscopy and ab initio molecular dynamics investigation, *Phys. Chem. Chem. Phys.*, 2014, 16(30), 16137–16144.
- 18 M. Ledinský, *et al.*, Raman Spectroscopy of Organic–Inorganic Halide Perovskites, *J. Phys. Chem. Lett.*, 2015, 6(3), 401–406.
- 19 R. G. Niemann, *et al.*, Halogen Effects on Ordering and Bonding of  $\text{CH}_3\text{NH}_3^+$  in  $\text{CH}_3\text{NH}_3\text{PbX}_3$  (X = Cl, Br, I) Hybrid Perovskites: A Vibrational Spectroscopic Study, *J. Phys. Chem. C*, 2016, 120(5), 2509–2519.
- 20 C. Quarti, *et al.*, The Raman Spectrum of the  $\text{CH}_3\text{NH}_3\text{PbI}_3$  Hybrid Perovskite: Interplay of Theory and Experiment, *J. Phys. Chem. Lett.*, 2014, 5(2), 279–284.
- 21 B. D. Fahlman and A. R. Barron, Substituent effects on the volatility of metal  $\beta$ -diketonates, *Adv. Mater. Opt. Electron.*, 2000, 10(3–5), 223–232.
- 22 A. Dualeh, *et al.*, Thermal Behavior of Methylammonium Lead-Trihalide Perovskite Photovoltaic Light Harvesters, *Chem. Mater.*, 2014, 26(21), 6160–6164.
- 23 Y. Liu, *et al.*, Two-Inch-Sized Perovskite  $\text{CH}_3\text{NH}_3\text{PbX}_3$  (X = Cl, Br, I) Crystals: Growth and Characterization, *Adv. Mater.*, 2015, 27(35), 5176–5183.
- 24 T. Supasai, *et al.*, Formation of a passivating  $\text{CH}_3\text{NH}_3\text{PbI}_3/\text{PbI}_2$  interface during moderate heating of  $\text{CH}_3\text{NH}_3\text{PbI}_3$  layers, *Appl. Phys. Lett.*, 2013, 103(18), 183906.

